1970

Shell Source Burning Stars with Highly Condensed Cores

S. Refsdal
University of Nebraska-Lincoln

A. Weigert
University of Nebraska-Lincoln

Astron. & Astrophys. 6, 426—440 (1970)

Shell Source Burning Stars with Highly Condensed Cores

S. Refsdal and A. Weigert
Behlen Laboratory of Physics, University of Nebraska
Institute of Theoretical Astrophysics, University of Oslo
Hamburger Sternwarte

Received February 10, 1970

Simple analytical relations are derived — similar to the homology relations for homogeneous stars — which describe the behaviour of shell source burning models with highly condensed cores. Many features which are known from evolutionary calculations (and partly from observations) of such stars can be understood as coming essentially from the increase of the mass M_c of the core.

Changes of the radius R_c of the core, of the radiation pressure, and of the chemical composition are also considered. For a comparison, sequences of numerically calculated equilibrium models are presented. They show that the analytical relations give, even quantitatively, good approximations to the numerical results.

Key words: stellar structure — stellar evolution

I. Introduction

In stellar evolutionary theory, one often encounters stellar models with a nuclear burning in a concentric shell source which surrounds a highly condensed core. Such models occur when a nuclear fuel has been exhausted in a central core of not too large mass; this core then has contracted and the electron gas has become degenerate by which the ignition of the next fuel is, for the moment, prevented. Such models show many peculiar properties and have caught considerable attention by several authors, see for instance Eggleton (1967).

The most important example for these shell source burning stars are the stars on the ascending branch of globular cluster diagrams. In this case the hydrogen burning shell source surrounds a degenerate helium core, and the phase under consideration is terminated when the helium flash starts at the top of this ascending branch.

(We will, as an example, concentrate mainly on this evolutionary phase of low massive stars, although the discussion applies also to quite different cases.)

Stars on the ascending branch evolve with steeply increasing luminosity (up to a factor of 10^3). The relatively large number of stars observed there indicates that it is essentially a nuclear phase while normally the (shorter) Kelvin-Helmholtz time scale is characteristic for the evolution between two central burnings. Numerical models for this phase show, in addition, that the central part of the star contracts while the outer layers expand; the mass ΔM_r contained in the shell source is steeply decreasing and this shell source remains always radiative. Moreover, calculations for mass loss of such stars (for binary evolution) show that the luminosity (and, in fact, the whole structure of the shell source region where this luminosity is generated) is in a wide range nearly independent of the mass in the envelope, i.e. *independent of the total mass of the star*. However, the physical understanding of these results of numerical calculations still seems to be unsatisfactory. In such a situation, a simple analytical description of the models can be very useful not only for interpreting the numerical results, but also for generalizing them. (The well known homology relations offer the best example for the use which one can make of such descriptions in other cases.)

The very important region inside and above the shell source will be analysed in the following chapter II. This region of the star is apparently influenced mainly by the highly condensed central core. Since practically no energy is flowing out of the core during this phase, the core can influence its surroundings only by its large gravitational potential Φ. In fact, while the radius of the core $R_c \ll R$ (radius of the star), the mass of the core M_c is a considerable fraction of M. Therefore, in the shell source $\Phi \approx \Phi_c \sim M_c/R_c$ is rather large. This leads us to try a discussion of this region in terms of M_c and R_c as given parameters. (This means, we treat formally the

central part as if it would be a hard core of radius R_c and mass M_c, the surface temperature of which is the same as the temperature in the bottom of the shell source.) Though R_c is formally treated as an independent parameter, it can be shown that an $M_c - R_c$ relation must exist for such models so that R_c will adjust according to any new value of M_c (see Appendix). Then, a sequence of models with gradually increasing M_c can represent an evolutionary sequence of a real star in which M_c grows due to the outwards burning of the shell source. The influence of changing radiation pressure and changing chemical composition are also treated.

The approach used here is very similar to that for deriving the usual homology relations. As well known, these homology relations are extremely useful for interpreting and generalizing the numerical results for *homogeneous* stars (or homogeneous parts of a star, for instance, a contracting core). In homology, the suitable independent variable is M_r and the parameter – varied from model to model – is R. For two models with R and R', one has $r(M_r)/r'(M_r) = R/R'$ for all M_r; and corresponding relations (with different powers of R/R') hold for the other functions as $P(M_r)$, $T(M_r)$ or $\varrho(M_r)$.

If we now look for a similar type of relations for the shell source region, it would be very inconvenient to take M_r as the independent variable or to express the changes from model to model in terms of R. However, simple relations are obtained if one uses r/R_c as independent variable; the changes of P, T, ϱ and L_r can be expressed then in terms of certain powers of M_c and R_c, for instance, $\varrho\,(r/R_c)/\varrho'\,(r'/R_c') = (M_c/M_c')^{\alpha_1} \cdot (R_c/R_c')^{\alpha_2}$ for all $r/R_c = r'/R_c'$ in the region under consideration.

Of course, as in the case of the homology relations, one has to prove by numerical calculations that the derived relations describe the behaviour of the models to a good approximation. For this purpose, several sequences of stellar models were calculated which are presented in chapter III. For simplicity, the sequences consist of equilibrium models; these are good approximations to the real evolutionary sequences of the phase in question except for the very last part of evolution just before the onset of the helium flash.

In the calculated sequences, M_c was varied from about 0.16 to 0.45 $M_\odot$. Furthermore, M was varied over a rather wide range (0.20 . . . 1.4 $M_\odot$). This was done not only to test the dependence (or independence) of the shell source region on M, but also for deriving numerical values and relations for the mass exchange

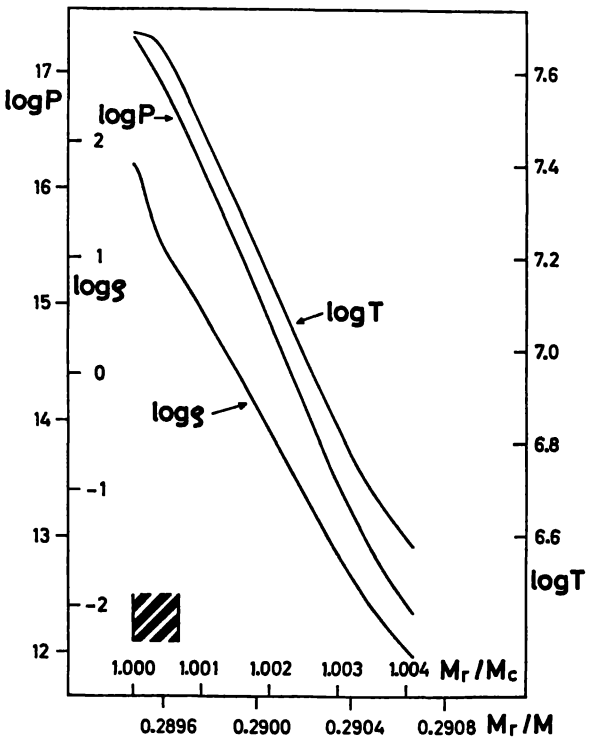

Fig. 1. The functions P (in dyne cm^{-2}), T (in °K) and ϱ (in g cm^{-3}) are plotted over M_r/M_c and over M_r/M for an equilibrium model of $M = 1.4\,M_\odot$. The curves cover the region inside and above the shell source. The stripped area indicates the extension of the shell source burning ($L_r/L = 0 \ldots 0.99$)

in close binary systems of low mass. The agreement between these numerical models and the analytical relations is satisfactory.

In the appendix, the relation between M_c and R_c is discussed. For this, the highly condensed central core is treated essentially as consisting of a "white dwarf". The main difference turns out to be that the so-called transition layer is here an isothermal layer of high temperature (the shell source temperature); this provides a much larger extension of this layer than in the case of a normal white dwarf.

II. Analytical Treatment

a) Assumptions and Basic Equations

Many numerical models are available in which a shell source surrounds a highly condensed core. If we examine such a model in the region inside and above the shell source, we find the following important behaviour of the relevant functions P, T and ϱ: from

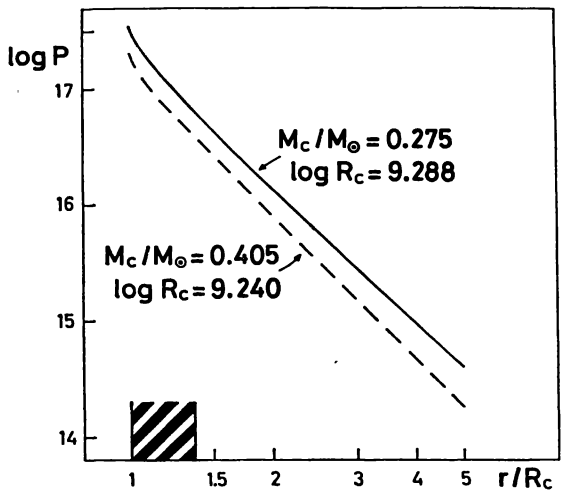

Fig. 2. For two equilibrium models of $M = 1.4\,M_\odot$, $\log P$ (P in dyne cm^{-2}) is plotted over r/R_c (R_c = core radius). The stripped area indicates the extension of the shell source burning ($L_r/L = 0 \ldots 0.99$)

the bottom of the shell source (i.e. from the surface of the central core) and outwards, these functions drop by several powers of 10 over a very small interval ΔM_r of the mass, such that $\Delta M_r \ll M_r$, or $M_r \approx M_c$ (mass of the central core) in this whole region. An example is given in Fig. 1, where $\log P$, $\log T$ and $\log \varrho$ are plotted over M_r for such a model. Consequently, the structure of the shell source region depends very little on the structure of most of the matter in the envelope.

One can now compare two models of different masses M_c, M_c' and radii R_c, R_c' of the core. If then the functions P and P', T and T' ... are plotted over r/R_c and r'/R_c', the differences $\Delta \log P$, $\Delta \log T$ ... between the two models in corresponding points ($r/R_c = r'/R_c'$) are nearly constant throughout and just above the shell source (see Fig. 2).

For the analytical treatment, we make the following simplifying assumptions which are fairly well fulfilled by the numerical solutions:

(1) we consider only the region from the bottom of the shell source, $r = R_c$, up to a point $r = r_0$ where P, T and ϱ have already decreased appreciably (and where, of course, $L_r = L$);

(2) we take $M_r = \text{const.} = M_c$ (mass of the core);

(3) we treat equilibrium models. This means that $dL_r/dM_r = \varepsilon_N$ so that $L_r = 0$ throughout the isothermal core and $L = L_{\text{shell}}$;

(4) we consider a perfect gas and allow for the presence of radiation pressure P_R;

$\psi = 1 - P_R/P$ can vary inside a model. If we, however, compare two models with core radii R_c and R_c', then ψ/ψ' should be constant in all corresponding points (i.e. for all $r/R_c = r'/R_c'$);

(5) the whole region is radiative;

(6) for two different models with core radii R_c and R_c' respectively, the ratios P/P', ϱ/ϱ', T/T' and L_r/L_r' are constant for all $r/R_c = r'/R_c'$. Furthermore we assume the X-profile (X = hydrogen content) to be "similar" in both models, i.e. $X/X_{\text{envelope}} = X'/X'_{\text{envelope}}$ for all corresponding points ($r/R_c = r'/R_c'$).

The basic equations which will be considered are: the equation of state and the equations for hydrostatic equilibrium, for radiative transport of energy, and for energy generation. We need only the proportionalities and write:

$$P \sim \frac{\varrho T}{\psi \mu}, \tag{1}$$

$$dP \sim M_c \varrho\, d\left(\frac{1}{r}\right), \tag{2}$$

$$d(T^4) \sim \varkappa \varrho\, L_r\, d\left(\frac{1}{r}\right) = \varkappa_0\, \varrho\, P^a\, T^b\, L_r\, d\left(\frac{1}{r}\right), \tag{3}$$

$$d\,L_r \sim \varepsilon_N\, \varrho\, d(r^3) = \varepsilon_0\, \varrho^n\, T^\nu\, d(r^3). \tag{4}$$

In Eqs. (3) and (4) we have used the expressions

$$\varkappa = \varkappa_0 \cdot P^a\, T^b, \tag{5}$$

$$\varepsilon = \varepsilon_0 \cdot \varrho^{n-1}\, T^\nu, \tag{6}$$

where $\varkappa_0$ and ε_0 will depend on the chemical composition, i.e. they are functions of r. In Eq. (2), M_r is replaced by M_c according to assumption (2). For the same reason we need not consider an equation for dM_r/dr. In Eq. (4), the term $\varepsilon_g = -T\frac{\delta S}{\delta t}$ is put equal to zero according to assumption (3).

b) *Changes of M_c and R_c*

As discussed in the introduction, we will here treat formally the mass and the radius of the core, M_c and R_c, as independent parameters which may vary from model to model. Thus, we certainly cover a much wider range of possible models than will actually occur, since there will exist a $M_c - R_c$ relation. In this section, ψ, μ, $\varkappa_0$ and ε_0 are assumed not to vary from model to model in corresponding points (although they can be functions of r inside one model). We will always use the independent

variable r/R_c which is suggested by assumption (6). The range under consideration is $r/R_c = 1 \ldots r_0/R_c$.

Let us think that a solution of the Eqs. (1)–(4) is known for a special pair of values M_c' and R_c', i.e. that ϱ', T', P', and L_r' are given as functions of r'/R_c'. We now try to find another solution ϱ, T, P, and L_r as functions of r/R_c for any other values M_c, R_c. Assumption (6) suggests to try the following relation for, say, ϱ:

$$\frac{\varrho(r/R_c)}{\varrho'(r'/R_c')} = \lambda = \left(\frac{M_c}{M_c'}\right)^{\alpha_1} \cdot \left(\frac{R_c}{R_c'}\right)^{\alpha_2} \tag{7}$$

for all $r/R_c = r'/R_c'$, and corresponding relations for T, P, and L_r. These relations may be briefly written in the following way:

$$\varrho\,(r/R_c) \sim M_c^{\alpha_1} \cdot R_c^{\alpha_2}\,, \tag{8}$$

$$T\,(r/R_c) \sim M_c^{\beta_1} \cdot R_c^{\beta_2}\,, \tag{9}$$

$$P\,(r/R_c) \sim M_c^{\gamma_1} \cdot R_c^{\gamma_2}\,, \tag{10}$$

$$L_r\,(r/R_c) \sim M_c^{\delta_1} \cdot R_c^{\delta_2}\,. \tag{11}$$

From Eqs. (8), (9), (10) and (1), it then follows that

$$\gamma_1 = \alpha_1 + \beta_1\,; \quad \gamma_2 = \alpha_2 + \beta_2\,. \tag{12}$$

By integration of Eq. (2), one gets the pressure P at any point r inside or just above the shell source:

$$P\,(r/R_c) = P\,(r_0/R_c) + \int_{1/r_0}^{1/r} G M_c\, \varrho\, d\left(\frac{1}{r}\right) \tag{13}$$

where we start at a point r_0 so far outside that $P\,(r_0/R_c) \ll P\,(r/R_c)$. ($G$ is the gravitational constant.) Then, with $x = R_c/r$,

$$P\,(r/R_c) = \frac{GM_c}{R_c} \cdot \int_{R_c/r_0}^{R_c/r} \varrho\, dx\,. \tag{14}$$

For the other model (with M_c', R_c') we can make a corresponding integration and eliminate ϱ' by using relation (7):

$$P'\,(r'/R_c') = \frac{GM_c'}{R_c'} \cdot \int_{R_c'/r_0'}^{R_c'/r'} \varrho'\, dx = \frac{GM_c'}{R_c'} \cdot \left(\frac{M_c'}{M_c}\right)^{\alpha_1} \cdot \left(\frac{R_c'}{R_c}\right)^{\alpha_2} \cdot \int_{R_c/r_0}^{R_c/r} \varrho\, dx \tag{15}$$

for $r_0/R_c = r_0'/R_c'$ and $r/R_c = r'/R_c'$. Eliminating the integral in Eqs. (14) and (15), we get

$$P\,(r/R_c) = P'\,(r'/R_c') \cdot \left(\frac{M_c}{M_c'}\right)^{\alpha_1+1} \cdot \left(\frac{R_c}{R_c'}\right)^{\alpha_2-1} \tag{16}$$

or briefly

$$P\,(r/R_c) \sim M_c^{\alpha_1+1} \cdot R_c^{\alpha_2-1}\,. \tag{17}$$

From this and Eq. (10) we find that

$$\gamma_1 = \alpha_1 + 1\,; \quad \gamma_2 = \alpha_2 - 1\,. \tag{18}$$

An integration and elimination similar to that in Eqs. (13)–(17) can be done for the transport Eq. (3). In fact, it can easily be seen from the exponents in Eq. (3) that this integration yields

$$T^{4-b} \sim M_c^{\alpha_1 + a\gamma_1 + \delta_1} \cdot R_c^{\alpha_2 + a\gamma_2 + \delta_2 - 1}\,. \tag{19}$$

Comparing the left side with Eq. (9), we get

$$\begin{aligned} (4-b)\,\beta_1 &= \alpha_1 + a\gamma_1 + \delta_1\,; \\ (4-b)\,\beta_2 &= \alpha_2 + a\gamma_2 + \delta_2 - 1\,. \end{aligned} \tag{20}$$

Finally, a similar integration of the energy Eq. (4) gives

$$L_r \sim M_c^{n\alpha_1 + \nu\beta_1} \cdot R_c^{n\alpha_2 + \nu\beta_2 + 3} \tag{21}$$

and comparing the left side with Eq. (11) one finds

$$\delta_1 = n\alpha_1 + \nu\beta_1\,; \quad \delta_2 = n\alpha_2 + \nu\beta_2 + 3\,. \tag{22}$$

We have now obtained the eight algebraic Eqs. (12), (18), (20) and (22) from which the eight exponents $\alpha_1, \alpha_2, \ldots, \delta_2$ can be found:

$$\left.\begin{aligned} &\alpha_1 = -\frac{\nu - 4 + a + b}{n + 1 + a}\,, \quad \alpha_2 = \frac{\nu - 6 + a + b}{n + 1 + a}\,, \\ &\beta_1 = 1\,, \qquad\qquad \beta_2 = -1\,, \\ &\gamma_1 = 1 - \frac{\nu - 4 + a + b}{n + 1 + a}\,, \\ &\gamma_2 = -1 + \frac{\nu - 6 + a + b}{n + 1 + a}\,, \\ &\delta_1 = \nu - n \cdot \frac{\nu - 4 + a + b}{n + 1 + a}\,, \\ &\delta_2 = -\nu + 3 + n \cdot \frac{\nu - 6 + a + b}{n + 1 + a}\,. \end{aligned}\right\} \tag{23}$$

Thus, we have derived a set of exponents for the relations (8)–(11) such that the basic Eqs. (1)–(4) are fulfilled.

It should be noted that only the equation of state and the condition for hydrostatic equilibrium are needed in order to determine the dependence of T on M_c and R_c ($\beta_1 = -\beta_2 = 1$ from Eqs. (12) and (18)).

Typical numerical values for the exponents are given in Section (g) of this chapter, after we have discussed changes of the radiation pressure and of the chemical composition.

It may be emphasized, however, that already the above results can give a surprisingly good understanding of many evolutionary features. This can be

easily understood: an evolutionary sequence for such models is essentially a sequence of increasing M_c, where the *relative* change of M_c is usually much larger than the relative change which one has to consider for other parameters; and the exponents of M_c ($\alpha_1 \ldots \delta_1$) can have rather large values. Thus, the effects which will be treated in the next sections in many cases add only corrections to the dominating effects coming from the increase of M_c.

c) Changes of the Radiation Pressure

For the moment let us forget that ψ (ratio of gas pressure to total pressure) depends explicitly on P and T, so that we formally can treat it as a free parameter. From one model to another, ψ is assumed to change by a constant factor in corresponding points. The procedure is similar to that in the foregoing section (but now M_c and R_c are constant). We try the relations:

$$\left.\begin{aligned} \varrho\,(r/R_c) &\sim \psi^{\alpha_3}\,, \\ T\,(r/R_c) &\sim \psi^{\beta_3}\,, \\ P\,(r/R_c) &\sim \psi^{\gamma_3}\,, \\ L_r\,(r/R_c) &\sim \psi^{\delta_3}\,. \end{aligned}\right\} \tag{24}$$

(Since $R_c = \text{const.}$, we could, of course, as well have dropped here the normalization of the independent variable.)

By integrating the basic Eq. (2), (3), (4) one gets

$$\left.\begin{aligned} P\,(r/R_c) &\sim \psi^{\alpha_3}\,, \\ T^{4-b}(r/R_c) &\sim \psi^{\alpha_3+a\gamma_3+\delta_3}\,, \\ L_r\,(r/R_c) &\sim \psi^{n\alpha_3+\nu\beta_3}\,. \end{aligned}\right\} \tag{25}$$

[Compare this with the analogous results (17), (19), (21) of the corresponding integrations in the foregoing section.]

Inserting the first two of Eqs. (24) into the equation of state (1), we obtain (for $\mu = \text{const.}$)

$$P\,(r/R_c) \sim \psi^{\alpha_3+\beta_3-1}\,. \tag{26}$$

By using Eq. (24), the left sides of Eqs. (25) and (26) can be expressed as powers of ψ. A comparison of the exponents gives four algebraic equations which can be solved:

$$\left.\begin{aligned} \alpha_3 &= -\frac{\nu-4+b}{n+1+a}\,,\ \beta_3 = 1\,, \\ \gamma_3 &= -\frac{\nu-4+b}{n+1+a}\,,\ \delta_3 = \nu - n\cdot\frac{\nu-4+b}{n+1+a}\,. \end{aligned}\right\} \tag{27}$$

For simultaneous changes of M_c, R_c and ψ, one has only to multiply the right sides of Eqs. (24) by the corresponding ones of Eqs. (8)–(11). Some typical numerical values for the exponents $\alpha_3, \ldots, \delta_3$ are given in Section g) of this chapter. It may be noted that any deviation from the perfect gas (such as the presence of radiation pressure) can be included in this whole analysis by using the general differential form

$$\frac{d\varrho}{\varrho} = \left(\frac{\partial \ln \varrho}{\partial \ln P}\right)_T \cdot \frac{dP}{P} + \left(\frac{\partial \ln \varrho}{\partial \ln T}\right)_P \cdot \frac{dT}{T} \tag{28}$$

as the equation of state.

d) Changes of the Chemical Composition

For simplicity, let us first assume that we can describe the change of the chemical composition from one model to another by a change of only μ (mean molecular weight), and that the relative change $\Delta \ln \mu$ is constant throughout the whole region. Then we treat μ as a new free parameter of the model. However, μ appears explicitly only in the basic Eq. (1), $P \sim \varrho T/(\psi\mu)$, in the same way as ψ does. A change of μ is thus completely equivalent to a change of ψ. (In fact, we could have treated in the last section the product $\psi \cdot \mu$ as a single parameter.) Consequently, the results for the changes of ψ can be used, and we have

$$\varrho \sim \mu^{\alpha_3},\ T \sim \mu^{\beta_3},\ P \sim \mu^{\gamma_3},\ L_r \sim \mu^{\delta_3} \tag{29}$$

where the exponents $\alpha_3 \ldots \delta_3$ are given by Eqs. (27).

This procedure means to assume that a change of the chemical composition can be completely described by scaling up the function $\mu\,(r/R_c)$ in the whole region with a constant factor. This is rather artificial, at least for the μ-value at the bottom of the shell source. In practice, one is normally interested in discussing changes of X (hydrogen content) rather than of μ. A reasonable way to change X is to scale up $X\,(r/R_c)$ by a constant factor throughout the whole region inside and above the shell source. This is obviously not equivalent to a constant $\Delta \log \mu$ in the shell source where X varies inside a model from 0 (at $r = R_c$) to the value X_0 in the outer layers. Instead, one would then have $\Delta \log \mu = 0$ at the bottom of the shell source, while a maximum value of $\Delta \log \mu$ is reached where $X = X_0$.

But also in this case of $\Delta \log X = \text{const.}$, the resulting changes of, say, L can well be estimated from the above formulae (which assume $\Delta \log \mu = \text{const.}$). One only has to take a proper *average* value $\Delta \log \mu = \log \mu - \log \mu'$ (which corresponds to the X-change in an average point) and assume this $\Delta \log \mu$ to be representative for the whole region. For example, a scaling up of the whole X-profile by a factor $\frac{0.7}{0.6}$ corresponds to roughly $\Delta \log \mu = -0.03$.

Usually, $\varkappa_0$ and ε_0 [Eqs. (5), (6)] will depend on X and are thus functions of r/R_c. A scaling up of $X(r/R_c)$ will require changes of $\varkappa_0$ and ε_0. This can be treated analytically, if we assume that the functions $\varkappa_0(r/R_c)$ and $\varepsilon_0(r/R_c)$ are also scaled up by a constant factor. This is very reasonable for $\varepsilon_0 \sim X$ or $\sim X^2$. However, since $\varkappa_0$ is usually not proportional to any power of X, one has the same situation as with changes of μ and some proper average value for $\Delta \log \varkappa_0$ must be used. In order to find the corresponding effects on the models, we now treat $\varkappa_0$ and ε_0 as independent parameters and write

$$\left.\begin{aligned} \varrho\,(r/R_c) &\sim \varkappa_0^{\alpha_4} \cdot \varepsilon_0^{\alpha_5}\,, \quad T\,(r/R_c) \sim \varkappa_0^{\beta_4} \cdot \varepsilon_0^{\beta_5}\,, \\ P\,(r/R_c) &\sim \varkappa_0^{\gamma_4} \cdot \varepsilon_0^{\gamma_5}\,, \quad L_r\,(r/R_c) \sim \varkappa_0^{\delta_4} \cdot \varepsilon_0^{\delta_5}\,. \end{aligned}\right\} \quad (30)$$

Using the same procedure as in the above sections (say, for the changes of M_c and R_c), we find:

$$\left.\begin{aligned} &\alpha_4 = \alpha_5 = \gamma_4 = \gamma_5 = -\frac{1}{n+1+a} \\ &\beta_4 = \beta_5 = 0\,, \\ &\delta_4 = -\frac{n}{n+1+a}\,;\ \delta_5 = 1 - \frac{n}{n+1+a}\,. \end{aligned}\right\} \quad (31)$$

The numerical examples in Section g) will show that the effects of changing $\varkappa_0$ and ε_0 can often be considered as corrections to the dominating effect coming from the change of μ.

e) Extension of the Shell Source Region

Let us define the shell source (subscript "s") to be the layer between the points with $L_r/L = 0$ to, say, $L_r/L = 0.9$ (or to any other fixed value near 1). This shell contains a mass ΔM_s and has a radial extension $\Delta r_s = r_s - R_c$.

Consider two models with r_s, R_c, and r_s', R_c' respectively. Then assumption (6) requires that L_r/L_r' is the same for all corresponding points $r/R_c = r'/R_c'$, i.e. also far outside where $L_r = L$. This means that in corresponding points $L_r/L_r' = L/L'$, or that $L_r/L = L_r'/L' = 0.9$ for $r_s/R_c = r_s'/R_c'$. Then $\Delta r_s/R_c = -1 + r_s/R_c = -1 + r_s'/R_c' = \Delta r_s'/R_c'$. The *relative* radial extension $\Delta r_s/R_c$ of the shell source remains constant. [This discussion shows also that the relation given in Eq. (11) holds for the total luminosity L as well.]

The extension in mass, ΔM_s, of the shell source can easily be evaluated

$$\Delta M_s = \int_{R_c}^{r_s} 4\pi \varrho r^2\, dr = \frac{4\pi}{3} R_c^3 \cdot \int_1^{r_s/R_c} \varrho \cdot d\,(r/R_c)^3\,. \quad (32)$$

In another model where M_c, R_c and ψ may be changed, we get by using Eqs. (7) and (24):

$$\Delta M_s' = \frac{4\pi}{3} R_c'^3 \cdot \int_1^{r_s'/R_c'} \varrho'\, d\,(r'/R_c')^3$$

$$= \frac{4\pi}{3} R_c'^3 \cdot \left(\frac{M_c'}{M_c}\right)^{\alpha_1} \cdot \left(\frac{R_c'}{R_c}\right)^{\alpha_2} \cdot \left(\frac{\psi'}{\psi}\right)^{\alpha_3} \cdot \int_1^{r_s/R_c} \varrho\, d\,(r/R_c)^3 \quad (33)$$

$$\Delta M_s \sim M_c^{\alpha_1} \cdot R_c^{\alpha_2+3} \cdot \psi^{\alpha_3}\,. \quad (34)$$

Very similar, the mass ΔM_r can be found which is contained in the whole region under consideration (i.e. from $r = R_c$ to $r = r_0$, cf. Eq. (13)). An integration as in Eqs. (32) and (33), however extended from $r/R_c = r'/R_c' = 1$ to $r_0/R_c = r_0'/R_c'$, gives obviously the same proportionalities as for ΔM_s:

$$\Delta M_r \sim M_c^{\alpha_1} \cdot R_c^{\alpha_2+3} \cdot \psi^{\alpha_3}\,. \quad (35)$$

f) Comparison with Numerical Models

As shown in the foregoing Sections b)–d), it is possible to derive a simple analytical description for the shell source region when starting from the assumptions in Section a) and using the basic Eqs. (1)–(4). Now we will check these assumptions by comparing the analytical results with strict numerical solutions. For this comparison we first use the sequences of numerical equilibrium models which are described in detail in Chapter III.

From the equilibrium sequence with $M = 1.4\ M_\odot$, we use the models with $M_c = 0.276\ M_\odot \ldots 0.448\ M_\odot$ ($M_c/M = 0.197 \ldots 0.320$). This whole range of M_c was divided into four intervals (Tables 1–3), since the value of ν changes over the whole range of M_c and the exponents of M_c, R_c, and ψ are very sensitive to ν. Table 1 contains characteristic values of the first and last model of each of the intervals. The subscript "50" indicates that the quantity is taken

Table 1. *Characteristic values as taken from 5 numerical models with $M = 1.4\ M_\odot$*
Subscript "50" means the point with $L_r = 0.5\ L$. R_c is given in cm, T_{50} in °K, P_{50} in dyne/cm²

M_c/M	$\log R_c$	ψ_{50}	$\log T_{50}$	$\log P_{50}$	$\log L/L_\odot$
0.1966	9.3179	0.986	7.5168	17.3214	2.124
0.2236	9.3100	0.970	7.5710	17.2106	2.565
0.2544	9.2958	0.940	7.6244	17.1199	2.971
0.2896	9.2727	0.889	7.6750	17.0584	3.324
0.3202	9.2474	0.837	7.7121	17.0381	3.558

Table 2. *Changes in the four intervals of* M_c (compare Table 1) ν, a and b [cf. Eqs. (5), (6)] are average values for an interval

M_c/M	$\Delta \log M_c$	$\Delta \log R_c$	$\Delta \log \psi_{50}$	ν	a	b
0.1966–0.2236	0.0558	−0.0079	−0.0070	14.76	0.11	−0.89
0.2236–0.2544	0.0561	−0.0142	−0.0137	14.16	0.08	−0.79
0.2544–0.2896	0.0562	−0.0231	−0.0240	13.58	0.06	−0.70
0.2896–0.3202	0.0437	−0.0253	−0.0264	13.13	0.05	−0.45

Table 3. *Changes of* $\log T_{50}$, $\log P_{50}$, and $\log L$ *in the four intervals of* M_c (compare Tables 1 and 2), *as taken from numerical models for* $M = 1.4\, M_\odot$ ("num") *and predicted by the analytical relations* ("an")

M_c/M	$\Delta \log T_{\rm num}$ $\Delta \log T_{\rm an}$	$\Delta \log P_{\rm num}$ $\Delta \log P_{\rm an}$	$\Delta \log L_{\rm num}$ $\Delta \log L_{\rm an}$
0.1966–0.2236	0.0542 0.0567	−0.1108 −0.1135	0.441 0.458
0.2236–0.2544	0.0534 0.0566	−0.0907 −0.0944	0.406 0.432
0.2544–0.2896	0.0506 0.0553	−0.0615 −0.0679	0.353 0.391
0.2896–0.3202	0.0371 0.0426	−0.0203 −0.0363	0.234 0.273

at the point where L_r is 50% of L. (For simplicity, the given value of R_c is also taken at that point.) The values of ν, a and b in Table 2 are arithmetic means from the first and the last model of the corresponding M_c-interval; and in each of these models, the values at $L_r/L = 0.5$ were taken to be representative.

The differences $\Delta \log M_c$, $\Delta \log R_c$ and $\Delta \log \psi$ between the first and the last model of the various intervals are given in Table 2, the corresponding differences $\Delta \log T_{50}$, $\Delta \log P_{50}$, and $\Delta \log L$ are given in Table 3 with subscript "num". On the other hand, these latter differences can be predicted from those in Table 2 by using Eqs. (8)–(11) and (24):

$$\left.\begin{aligned}
\Delta \log T_{50} &= \beta_1 \Delta \log M_c \\
&\quad + \beta_2 \Delta \log R_c + \beta_3 \Delta \log \psi_{50}, \\
\Delta \log P_{50} &= \gamma_1 \Delta \log M_c \\
&\quad + \gamma_2 \Delta \log R_c + \gamma_3 \Delta \log \psi_{50}, \\
\Delta \log L &= \delta_1 \Delta \log M_c \\
&\quad + \delta_2 \Delta \log R_c + \delta_3 \Delta \log \psi_{50},
\end{aligned}\right\} \quad (36)$$

where the coefficients $\beta_1 \ldots \delta_3$ are calculated from Eqs. (23) and (27). The results are given in Table 3 with subscript "an". A comparison of the "numerical" with the "analytical" values in Table 3 gives, in general, a surprisingly good agreement. The largest discrepancy is: in the first interval 4%, in the second interval 6%, and in the third interval 10%. In the last interval (which extends very close to the He-flash!) we see that the approximations become worse; the changes in temperature and luminosity are still fairly well predicted by the analytical treatment (better than 15%), while the discrepancy for $\Delta \log P_{50}$ is 44%. This much larger discrepancy is easy to understand since, according to Eq. (36), the value of $\Delta \log P_{50}$ is a difference between larger quantities. Especially the radiation pressure causes some uncertainty because ψ is assumed to change from one model to another by a constant factor in all corresponding points. This is not any more a good approximation in the last models of the sequence. Much better agreement could be obtained if some average value $\bar{\psi}$ over the whole region had been used in Eq. (36) rather than ψ_{50}. It should be noted that the influence of variable $\varkappa$ (coming from $a \neq 0$, $b \neq 0$) is only a correction term, especially for the L-values. It is clear that the agreement will be good for the changes of ϱ, if those for P and T are satisfactory.

One basic assumption is that the functions ϱ, P, T, and L_r are only scaled up by constant factors in corresponding points ($r/R_c = r'/R_c'$). This was already illustrated for P in Fig. 2. The scaling up of L_r means that the relative extension of the shell source $\Delta r_s/R_c$ remains constant (see Section e)). In the range $M_c/M = 0.1966 \ldots 0.3202$ the numerical models show a change of $\Delta r_s/R_c$ from 0.166 to 0.183, i.e. of about 10%. Most of this total change occurs in the first of the intervals in Table 1. For $M_c/M = 0.2236$ to 0.3202, for example, $\Delta r_s/R_c$ changes only by 3%.

In the whole M_c-range in Table 1, the mass contained in the shell source changes by a factor 5.3.

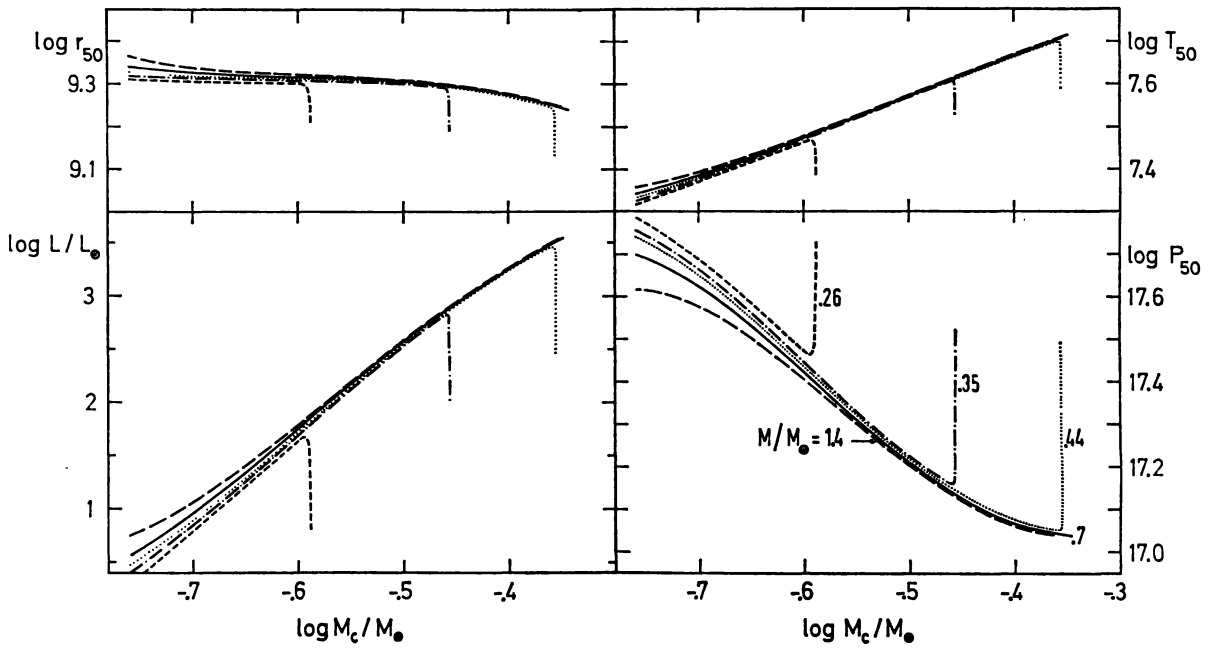

Fig. 3. For the equilibrium sequences with $M/M_\odot = 0.26$, 0.35, 0.44, 0.7 and 1.4, several functions are plotted over $\log M_c/M_\odot$ (M_c = mass of the core). The subscript "50" indicates that the quantity is taken at the point in the shell source where $L_r/L = 0.5$. The units are: r_{50} in cm, T_{50} in °K, P_{50} in dyne cm^{-2}. All curves for the same sequence (i.e. the same M) are plotted in the same way (for instance, all dotted curves correspond to $M/M_\odot = 0.44$)

This is in good agreement with an analytical prediction based on Eq. (34).

Another important assumption for the analytic description is that properties of the shell source region do not depend on the bulk of matter in the outer envelope. This means, for given M_c and R_c, we should find the same values of P_{50}, T_{50} and L for very different total masses M of the star, i.e. independent of $M_{\rm env} = M - M_c$. (Clearly, this assumption must break down for such small $M_{\rm env}$ that the surface comes near to, or even into the range over which the integrations, for instance, in Eq. (13) are extended.) Let us compare numerical models of the same core mass, $\log M_c/M_\odot = -0.5$, however with total masses of $M = 1.4\,M_\odot$ and $M = 0.35\,M_\odot$. The corresponding masses of the envelope, $M_{\rm env} = M - M_c$, are $1.05\,M_\odot$ and $0.034\,M_\odot$. In this large range of $M_{\rm env}$, we find the following small differences: $\Delta \log L = -0.05$, $\Delta \log T_{50} = -0.005$, $\Delta \log P_{50} = 0.02$. Such small changes (for a decrease of $M_{\rm env}$ by a factor 32) can be obtained by decreasing, at M = const., the mass of the core by only about 2% from $\log M_c/M_\odot = -0.50$ to -0.51. The effect the total mass M has on the shell source region can be seen from Fig. 3. There the dependence of T_{50}, P_{50}, L and r_{50} are plotted over M_c for very different values of M. Fig. 3 shows that the influence of M on these quantities decreases with increasing M_c. This could be expected since ΔM_r (the mass in the layer under consideration) decreases with increasing M_c. For lower M the curves have a sharp turn-off from those of larger M. This turn-off occurs where nearly $M_c \approx M$, i.e. where $M_{\rm env}$ is not any more large compared with ΔM_r. Then, of course, our assumptions must break down and the shell source must be affected by the surface values. From the numerical models one can learn that this does not happen before roughly $M_{\rm env} \approx 8 \cdot \Delta M_s$ (mass in the shell source). Since ΔM_s goes steeply down with increasing M_c, it is also clear that the turn-off will occur the closer to the limit $M_c = M$, the larger M is.

Now the question remains whether the assumption of equilibrium models is very restrictive, i.e. whether also real evolutionary models can be well approximated by the above analysis. Such an evolutionary sequence was calculated for a star of $M = 1.4\,M_\odot$ up to the He-flash. We now compare this star (subscript "real") with equilibrium models of $M = 1.4\,M_\odot$ (subscript "eq."). For a given value of M_c, $L_{\rm real}$ is always smaller than $L_{\rm eq}$, as can be

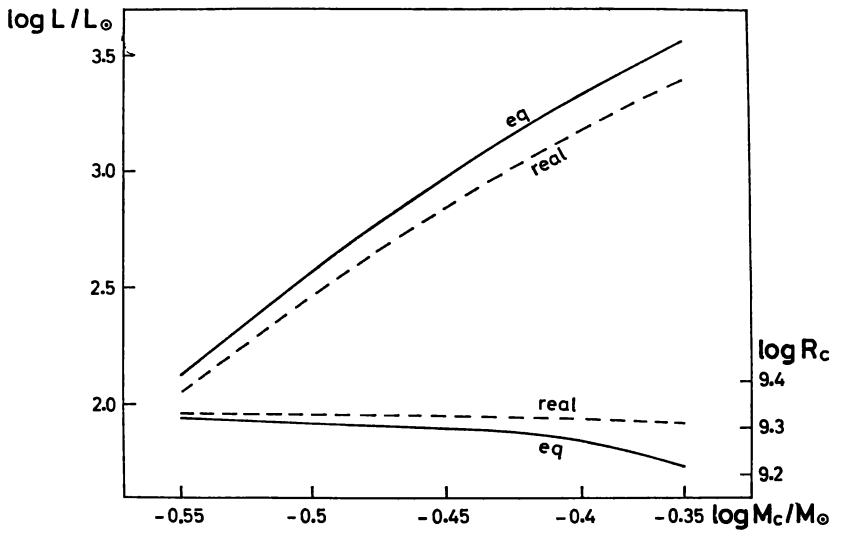

Fig. 4. For a star of $M = 1.4\,M_\odot$ the luminosity L and the radius R_c (in cm) of the core are plotted over the mass M_c of the core. Solid lines: equilibrium models; dashed lines: normal evolutionary calculations

seen from Fig. 4. The main reason for this difference in L is that $R_{c,\,\mathrm{real}} > R_{c,\,\mathrm{eq}}$ although some effect comes also from differences of the radiation pressure (see Fig. 4). For $\log M_c/M_\odot = -0.56$ we find from the numerical calculations a difference $\Delta \log R_c = \log (R_{c,\,\mathrm{eq}}/R_{c,\,\mathrm{real}}) = -0.0127$ and a corresponding difference $\Delta \log \psi_{50} = -0.001$. With these values the formulae of the above sections predict $\Delta \log L = \log (L_{\mathrm{eq}}/L_{\mathrm{real}}) = 0.079$, while the numerical models show that $\Delta \log L = 0.074$. For $\log M_c/M_\odot = -0.392$, we have $\Delta \log R_c = -0.0463$ and $\Delta \log \psi_{50} = -0.0144$, for which the formulae give $\Delta \log L = 0.167$, while the numerical models show $\Delta \log L = 0.155$. Therefore, the differences in luminosity between equilibrium models and real evolutionary models are well predicted from the analytical treatment if we take into account, especially, that $R_{c,\,\mathrm{real}} > R_{c,\,\mathrm{eq}}$.

One can understand, at least qualitatively, why $R_{c,\,\mathrm{real}} > R_{c,\,\mathrm{eq}}$ for a given M_c. The main reason is that, for equilibrium models, $L_c = 0$ (luminosity of the core) while for real models $L_c > 0$. This causes an increase of T from the bottom of the shell source towards the center. Therefore, the non-degenerate outer layers of the core have a higher temperature and, thus, a larger radial extension in a real model.

It should be pointed out that the difference $\Delta \log L$ between equilibrium and real models is not large compared to the increase of $\log L$ over the whole range of M_c. For a change of $\log M_c$ by only about 0.02 in the equilibrium sequences, one gets a change of $\log L$ which is equal to $\Delta \log L$. The main point is that, for a given M_c, the slopes of the two curves in Fig. 4 are nearly equal.

Summarizing, one can say that the predictions of the analytical treatment are in satisfactory agreement with the numerical results. This indicates that the assumptions on which the analytical treatment is based are reasonably chosen.

g) Examples, Discussion

In Table 4, some numerical examples can be found for the exponents describing the dependency of ϱ, T, P and L_r (α_j, β_j, γ_j and δ_j) on the most important parameters M_c, R_c, and ψ ($j = 1, 2$ and 3). Different values of ν and n were treated to show how the exponents vary with these quantities; for simplicity, $a = b = 0$ was taken in all cases. (The actual values of a and b would have added fairly small corrections.) The examples chosen can be representative for: CNO-cycle at high temperature ($\nu = 13$, $n = 2$) and at lower temperature ($\nu = 16$, $n = 2$); pp-reaction ($\nu = 4$, $n = 2$); triple α-reaction ($\nu = 22$, $n = 3$). Some of the exponents $\alpha_j \ldots \delta_j$ have quite different values for the different reactions. However, it is interesting to note that the β_j are independent of ν, n, a and b. The slopes of the curves in Fig. 3 depend, of course, on the exponents $\alpha_1 \ldots \delta_1$, although generally also the other exponents

Table 4. *For some values of ν and n and for $a = b = 0$, numerical values of the exponents are given as calculated from* Eqs. (23) *and* (27)

	α_j	β_j	γ_j	δ_j	
$j=1$	−3	1	−2	7	$\nu = 13$
$j=2$	2.33	−1	1.33	−5.33	$n = 2$
$j=3$	−3	1	−3	7	
$j=1$	−4	1	−3	8	$\nu = 16$
$j=2$	3.33	−1	2.33	−6.33	$n = 2$
$j=3$	−4	1	−4	8	
$j=1$	0	1	1	4	$\nu = 4$
$j=2$	−0.67	−1	−1.67	−2.33	$n = 2$
$j=3$	0	1	0	4	
$j=1$	−4.5	1	−3.5	8.5	$\nu = 22$
$j=2$	4	−1	3	−7	$n = 3$
$j=3$	−4.5	1	−4.5	8.5	

(other j) can play a role. This is because also R_c and ψ can change if we go from one value of M_c to another in this diagram. However, the changes of ψ and R_c (cf. Fig. 4) can often be neglected, and then the main changes of the model come from changes of M_c. So let us discuss now for simplicity only the dependencies on M_c. Typical average values for the whole range of M_c in Table 2 are: $\nu = 14$, $n = 2$, $a = 0.1$, $b = -0.8$, which give from Eqs. (8)–(11) and (23)

$$\varrho \sim M_c^{-3};\ T \sim M_c;\ P \sim M_c^{-2};\ L_r \sim M_c^{8}. \quad (38)$$

The most striking result is the steep increase of L_r (and thus also of L) with M_c. Increases of M_c by more than a factor 2 can easily occur in the evolution of such stars; this explains, for instance, the increase of L by several powers of 10 on the ascending branch of globular cluster diagrams. Another example is offered by the steeply increasing L with growing mass of the C–O core of more massive stars after central helium burning (Kippenhahn *et al.*, 1965).

Such a phase is essentially a nuclear phase and can last for a long time, especially if L is not too large and if hydrogen is burning in the shell source. This explains the relatively large number of stars which are observed on the ascending giant branch of globular cluster diagrams.

The increase of L is, of course, caused by the increase of T in the shell source by which the decrease of ϱ is easily overcome ($\varepsilon \sim \varrho^{n-1} \cdot T^{\nu}$, $\nu > n$). This increase of T with growing M_c contributes considerably to the ignition of helium at the end of this phase: the degenerate core is, for a long time, nearly isothermal and kept at the temperature T_s of the shell source. The increase of $T_s \sim M_c$ rises the temperature of the core by $\Delta \log T \approx 0.3 - 0.4$ up to more than $\log T = 7.7$. The additional increase to $\log T \approx 8$ (ignition temperature of helium) is due to the T-gradient which is built up in the transition layer of the core due to $L_{\text{core}} \neq 0$.

In the phase under consideration the central part of the core behaves like a white dwarf of increasing mass M_c, i.e. the central density increases. According to Eq. (38), however, ϱ decreases with increasing M_c inside and above the shell source so that the layers above the core expand. Thus, we have a special case of the so-called "mirror-principle" which was often encountered in calculations on stellar evolution: the core contracts while the layers above the shell source expand.

In general, one cannot conclude from this analysis of the shell source region how the total radius R of the star changes. In most parts of the phase under consideration, however, we are in a fortunate situation since the star is near the Hayashi-line in the H–R diagram. Then, one can roughly take $d \ln T_{\text{eff}} \approx 0$ and derive the R-change from the changes of L ($L \sim R^2 T_{\text{eff}}^4$)

$$d \ln R = \frac{1}{2} d \ln L = 4 \cdot d \ln M_c \quad (39)$$

[where the exponent $\delta_1 = 8$ is taken from Eq. (38)].

This increase of R, however, will not continue when the shell source comes close to the surface. According to Eq. (38), $\varrho \sim M_c^{-3}$ above the core. It seems reasonable to assume that the *average density*, $\bar{\varrho}$, of the whole envelope also decreases with a certain power of M_c, i.e. $\bar{\varrho} \sim M_c^{-\alpha}$, $\alpha > 0$. Now we have $\bar{\varrho} \sim M_{\text{env}}/R^3$, since $R \gg R_c$. With $d \ln M_c = (1 - M/M_c) \times d \ln M_{\text{env}}$, one can easily write down the changes of R:

$$d \ln R = \frac{\alpha}{3} \left(1 + \frac{1}{\alpha} \cdot \frac{1}{1 - M/M_c}\right) \cdot d \ln M_c\,. \quad (40)$$

For a given α and for $d \ln M_c > 0$, $d \ln R$ changes sign and becomes negative when M_c/M comes close enough to 1. (The corresponding decrease of R after a maximum can be seen for the equilibrium sequences in Fig. 5 where they bend over to the left in the H-R diagram.)

It is known from many evolutionary calculations that the mass ΔM_s contained in a shell source is steeply decreasing with progressive evolution. From Eq. (34), we obtain for the above example ($\nu = 14$,

$n = 2$, $a = 0.1$, $b = -0.8$, R_c = const., ψ = const.) $\Delta M_s \sim M_c^{-3}$. We would like to point out once more that the relative *radial* extension of the shell source remains constant (compare the beginning of Section e). Therefore, we cannot expect the shell source of such an evolving model to become thermally unstable due to a small radial extension (Schwarzschild and Härm, 1965), unless additional basic changes occur in the shell source region. (For example, the shell source was found to get this type of instability when it approached another shell source or the star's surface; Weigert, 1966; Kippenhahn *et al.*, 1968).

As shown in Eq. (35), the same proportionalities hold for ΔM_r (mass in the whole region under consideration) as for ΔM_s: with increasing M_c, ΔM_r decreases as M_c^{-3} for constant R_c and ψ. If the assumption (2) is approximately fulfilled for one model, it will become a gradually better approximation when the model evolves and M_c increases. ΔM_r was defined as the mass in the region over which the integration in Eq. (13) is extended, i.e. the region in which P drops by a certain, large enough factor. If ΔM_r decreases according to Eq. (35), then the same decrease must be found in the "pressure scale mass" $-dM_r/d\ln P$. In fact, from the equation of hydrostatic equilibrium ($dP/dM_r \sim M_r/r^4$) and with Eqs. (10) and (12), one gets

$$-\frac{dM_r}{d\ln P} \sim \frac{r^4}{M_r} P \sim M_c^{\gamma_1 - 1} \cdot R_c^{\gamma_2 + 4} = M_c^{\alpha_1} \cdot R_c^{\alpha_2 + 3} \sim \Delta M_r \,. \tag{41}$$

The large gravitational field produced by the core makes this "scale mass" rather small and provides thus the independency of the shell source region from the bulk of matter in the envelope. For the assumption (2) to be valid, one should rather have a small *relative* increase of M_r in the whole region. So it is better to look at the quantity

$$-\frac{d\ln M_r}{d\ln P} \sim \frac{r^4}{M_r^2} P \sim \frac{P}{g_c^2} \sim M_c^{\gamma_1 - 2} \cdot R_c^{\gamma_2 + 4} \sim \frac{\Delta M_r}{M_c} \tag{42}$$

where $g_c = GM_c/R_c^2$. It can easily be seen that the corresponding expressions which give the relative M_r-increase for a drop of T or ϱ by a factor e vary as $d\ln M_r/d\ln P$:

$$\frac{d\ln M_r}{d\ln P} \sim \frac{d\ln M_r}{d\ln T} \sim \frac{d\ln M_r}{d\ln \varrho} \,. \tag{43}$$

These quantities are interesting for the question as to whether the region under consideration will remain radiative when M_c is growing. From Eq. (43),

$$\nabla = \nabla_r = \frac{d\ln T}{d\ln M_r} \cdot \frac{d\ln M_r}{d\ln P} = \text{const.}, \tag{44}$$

i.e. ∇_r does not change with changing M_c and R_c. However, ∇_{ad} is a function of the radiation pressure:

$$\nabla_{ad} = \frac{2}{5} \cdot \frac{1 + 3(1-\psi)}{1 + 6(1-\psi) - \frac{3}{5}(1-\psi)^2} \tag{45}$$

where $1 - \psi \sim T^4/P$, as in the foregoing sections. Using Eqs. (9), (10) and (23), we can write

$$1 - \psi \sim \frac{T^4}{P} \sim M_c^{4-\gamma_1} \cdot R_c^{-4-\gamma_2} = \left(\frac{M_c}{R_c}\right)^{\gamma_2 + 4} M_c^{\frac{2}{n+1+a}} \tag{46}$$

For the example $\nu = 14$, $n = 2$, $a = 0.1$, $b = -0.8$,

$$1 - \psi \sim \left(\frac{M_c}{R_c}\right)^{5.35} \cdot M_c^{0.65} \,. \tag{47}$$

Thus, $1 - \psi \sim P_r/P$ is steeply increasing with increasing M_c. Hence ∇_{ad} is decreasing and the region comes closer to convective instability since ∇_r = const. In fact, the numerical models show that, with increasing M_c, the lower border of the convection zone approaches the shell source.

The total mass M of the star does not enter into the present description of the shell source region. Nevertheless, one can derive predictions for some surface values of the star: for L and, under the above mentioned conditions, also for R. This means that L and R are nearly independent of M. By this one can easily explain numerical results which were obtained for the evolution in close binary stars of low mass (Refsdal and Weigert, 1969; Giannone *et al.*, 1970). Even if a star in such a phase loses an appreciable amount of mass to its more massive companion, the star seems to be very little affected; it continues to increase L and R slowly (just as it would have done without mass loss). Thus more mass is shifted over the critical Roche lobe, although this Roche lobe expands. The mass loss does not stop until practically the whole envelope is stripped off. This behaviour can now easily be explained: the values and increases of L and R are only regulated by the core, the mass of which increases on a nuclear time scale; and L and R must continue to increase as long as our basic assumptions are valid. They can be expected to break down only if the shell source comes very close (in a mass scale) to the surface, or if the helium flash starts. (It may be noted that the

present analysis allows even quantitative predictions about the results of such type of binary evolution as will be shown in a forthcoming paper.)

Instead of having a M-L relation as for main-sequence stars, we have here rather a M_c-L relation. This can, in principle, give rise to other peculiar properties of such models: by increasing M for M_c = const. (for instance, by a rapid mass gain from a close companion), the star can drop *below* the M-L relation for main-sequence stars since its L-value will remain about constant. For example, such an "under-luminosity" occurs, according to rough estimates, for $M_c/M_\odot = 0.27$ and $M/M_\odot \gtrsim 3.3$.

For discussing changes of μ, we will again use the values $\nu = 14$, $n = 2$, $a = 0.1$, $b = -0.8$. Then, according to Eqs. (29) and (27),

$$\varrho \sim \mu^{-2.97},\ T \sim \mu,\ P \sim \mu^{-2.97},\ L_r \sim \mu^{8.06}. \quad (48)$$

Thus, the luminosity increases steeply with μ, as is also well known for much simpler models. For a change of $\Delta \log \mu = 0.03$ (compare section d), one obtains $\Delta \log L = 0.24$.

As described in Section (d), a change of μ will come from changes of X which normally imply simultaneous changes of ε_0 and $\varkappa_0$. For example, a hydrogen burning in the CNO-cycle means $\varepsilon_0 \sim X$. In this case, ν is relatively large and L is very sensitive to changes of μ ($\delta_4 = 8.06$ in Eq. (48)); compared to this, the effects of changing $\varkappa_0$ and ε_0 are small corrections. With $n = 2$, $a = 0.1$, we get from Eqs. (30) and (31): $L \sim \varkappa_0^{-0.645} \cdot \varepsilon_0^{0.355}$. Thus, increasing X results in decreasing L, since the effect from the decrease of μ is dominating. Such a drop of L is known from several evolutionary calculations in which the shell source moved over a chemical discontinuity so that X was increased in the shell source region (cf. Thomas, 1967). In calculations on binary evolution, such a decrease of L can result in an interruption of the mass exchange since also R decreases (Kippenhahn *et al.*, 1967; Refsdal and Weigert, 1969).

The situation can be more complicated in the case of p-p reactions where the values of ν and δ_3 are much smaller, while $\varepsilon_0 \sim X^2$.

In the present description, the quantities M_c, R_c, ψ, μ, $\varkappa_0$ and ε_0 are treated as free parameters, such that any one of them can be changed without changing the others. In reality, this is not true (as was already mentioned for M_c and R_c) since there will exist relations between the parameters. This gives rise to certain feed-back effects which normally result in small corrections only. Let us discuss the situation for changes of μ, ε_0 and $\varkappa_0$ and their effects on L.

Consider a $\delta\mu > 0$ which directly gives $\delta L > 0$ from Eqs. (29) and (27) ($\delta_3 > 0$). But then also $\delta T > 0$ and $\delta P < 0$ (since $\beta_3 > 0$, $\gamma_3 < 0$). An increase of T and a decrease of P just above the core will obviously affect the parameters R_c and ψ such that $\delta R_c > 0$, $\delta\psi < 0$. Both these changes give $\delta L < 0$ [Eqs. (24), (27), (11), (23)], which reduces somewhat the direct increase of L obtained from Eqs. (29) and (27).

A similar situation is found for $\delta\varepsilon_0 > 0$ and for $\delta\varkappa_0 > 0$, which also induce $\delta R_c > 0$, $\delta\psi < 0$. This again results in $\delta L < 0$, which means that the *direct* effect is increased for the case of $\delta\varkappa_0 > 0$ (since then $\delta L < 0$ already from Eqs. (30), (31)).

III. Sequences of Equilibrium Models

For 6 values of the stellar mass M, sequences were calculated of shell source burning models with highly condensed He-cores. The values of M are: $M/M_\odot$ = 0.2, 0.26, 0.35, 0.44, 0.7 and 1.4. Each model consists of a He-core of mass M_c, and of a hydrogen rich envelope of mass M_{env} ($M = M_c + M_{\text{env}}$).

In any of the sequences, M is kept constant, while M_c is varying. The lowest M_c-values are about 0.17 $M_\odot$. M_c is allowed to increase very near to $M_c = M$ for the sequences with $M/M_\odot$ = 0.2, 0.26, 0.35 and 0.44. The sequences for $M/M_\odot = 0.7$ and 1.4 are stopped when $M_c \approx 0.45\ M_\odot$. (At about this value of M_c the He-flash will start in a real star of the same chemical composition.)

The chemical composition of the outer envelope is $X = 0.602$, $Y = 0.354$, $Z = 0.044$; in the core, $X = 0$, $Y = 0.956$, $Z = 0.044$. In the lowest part of the envelope, X varies from 0 to $X_0 = 0.602$. This X-profile is arranged such that $X/X_0 = L_r/L$. (A profile very near to the assumed one is found to be produced by the shell source burning in similar stars which are evolving towards the He-flash. The exact form of the profile has anyway no large effect on such integral quantities as the luminosity.)

In this region just above the core a hydrogen burning shell source produces the star's luminosity. The models are assumed to be in thermal equilibrium, i. e. $\dot{P} = \dot{T} = 0$ is taken in the equation of energy. Since there is no nuclear burning in the core, one has then $L_c = 0$, and the core is isothermal with $T = T_c$ = temperature at the bottom of the shell source. The density in the core is rather high and the electron

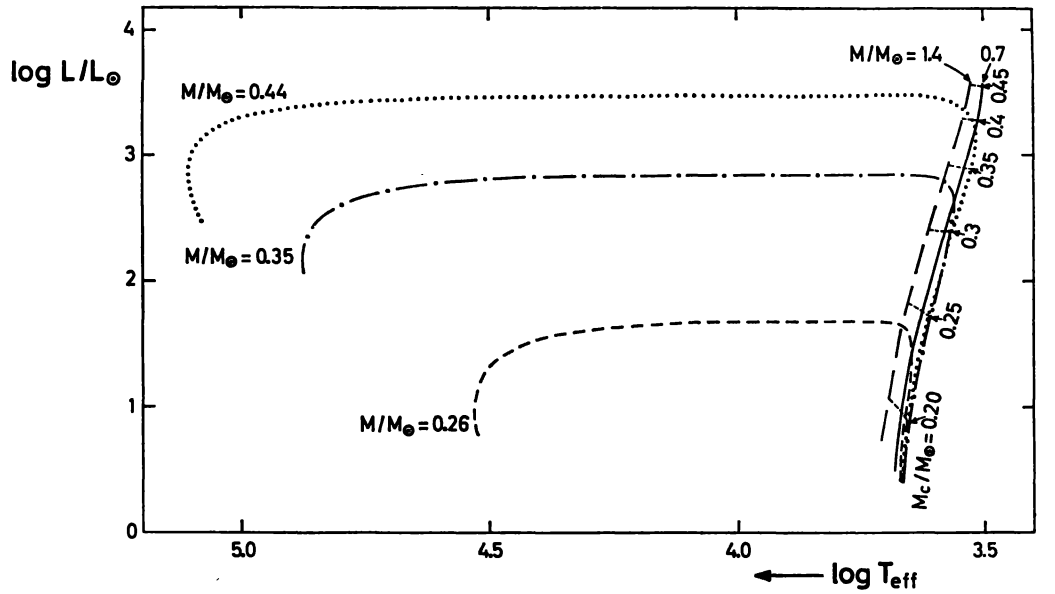

Fig. 5. HR-diagram for the equilibrium sequences of $M/M_\odot = 0.26$, 0.35, 0.44, 0.7 and 1.4. In the right part of the diagram, some additional lines connect the points of M_c = const. on the different sequences

gas is degenerate in most parts. This provides the pressure for supporting the weight of the envelope.

Such an equilibrium model can easily be obtained by starting from normal evolutionary calculations: for a certain moment of the evolution (i.e. for a certain M_c) one only has to cut off artificially in the computer program any change of the chemical composition and to take $\varepsilon_g = -T \cdot \partial S/\partial T = 0$. (Even without the latter condition, the model soon settles down to the equilibrium state, once the core mass does not increase any more.) It is then easy to obtain, for instance, other equilibrium models for the same M but different M_c. Except for the indicated changes, the computer program used here is that described by Hofmeister *et al.* (1967).

The position of the sequences in the H-R diagram is shown in Fig. 5. Numerical values for selected models can be taken from Table 5. As long as M_c is considerably smaller than M, the sequences are near the Hayashi-line, and L is increasing with M_c. When M_c comes close to M (i.e. when $M_{\rm env}$ becomes small), the sequences go far to the left in the H-R diagram before they finally bend downwards.

When the sequences of smaller M turn to the left in the H-R diagram, R is sharply reduced with increasing M_c. An appreciable drop of L does not occur before R is already down to roughly $10\,R_c$. This shows that the shell source (where L is produced) is practically not affected by layers which are farther outwards than about $10\,R_c$.

Appendix
On the $M_c - R_c$ Relation

We will here indicate how one can, in principle, obtain the relation between R_c and M_c for equilibrium models. For this, one has to consider the structure of the condensed core. A difficulty is that the degeneracy of the electron gas varies continuously from the center to the surface. Therefore, very similar to the usual theory of white dwarfs, we divide the core into an interior part of high degeneracy ("white dwarf") and a "transition layer" of negligible degeneracy. This latter region may extend from $r = r_d$ to $r = R_c$. For simplicity, let us assume that this region contains a negligible part of the mass M_c, i.e. $M_d \approx M_c$. For the equilibrium models which will be considered one has T = const. $= T_c$ throughout the whole core. (This is, by the way, also a fairly good approximation for many evolutionary models since $\Delta \log T$ between center and shell source becomes appreciable only near the onset of the helium flash.)

Now we consider an integration inwards through the transition layer, starting from $r = R_c$. As outer boundary conditions, one has the values at the

Table 5. *Some models of the equilibrium sequences*

$M/M_\odot$	M_c/M	$M_c/M_\odot$	$\log L$	$\log T_{\rm eff}$
1.4	0.1250	0.175	0.768	3.709
1.4	0.1357	0.19	0.935	3.700
1.4	0.1786	0.25	1.758	3.657
1.4	0.2427	0.34	2.829	3.583
1.4	0.3072	0.43	3.465	3.532
0.7	0.2500	0.175	0.562	3.681
0.7	0.2714	0.19	0.803	3.674
0.7	0.3572	0.25	1.742	3.626
0.7	0.4854	0.34	2.810	3.542
0.7	0.6144	0.43	3.452	3.507
0.44	0.3980	0.175	0.480	3.67
0.44	0.4315	0.190	0.732	3.663
0.44	0.5680	0.250	1.711	3.613
0.44	0.7725	0.340	2.797	3.534
0.44	0.8943	0.3935	3.218	3.518
0.44	0.9388	0.4130	3.343	3.528
0.44	0.99776	0.4390	3.473	3.871
0.44	0.99906	0.4396	3.373	3.916
0.44	0.99954	0.4398	2.853	5.105
0.44	0.99958	0.4398	2.471	5.079
0.35	0.500	0.175	0.417	3.667
0.35	0.543	0.190	0.688	3.661
0.35	0.714	0.250	1.687	3.609
0.35	0.9093	0.3180	2.564	3.561
0.35	0.9725	0.3405	2.779	3.573
0.35	0.9931	0.3476	2.840	3.830
0.35	0.99690	0.3489	2.740	4.675
0.35	0.99842	0.3494	2.212	4.874
0.26	0.6730	0.175	0.330	3.675
0.26	0.7310	0.190	0.615	3.670
0.26	0.9168	0.2385	1.450	3.649
0.26	0.9600	0.2495	1.620	3.660
0.26	0.9791	0.2546	1.680	3.882
0.26	0.9879	0.2569	1.580	4.347
0.26	0.9929	0.2582	1.006	4.528
0.20	0.7000	0.140	−0.422	3.689
0.20	0.8750	0.175	0.190	3.719
0.20	0.9162	0.1832	0.326	3.736
0.20	0.9460	0.1892	0.392	3.793
0.20	0.9644	0.1929	0.292	4.065
0.20	0.9778	0.1955	−0.313	4.200

bottom of the shell source $\varrho = \varrho_c$, $T = T_c$, $P = P_c$. For these, the relations must hold which were derived in Chapter II, i.e. we have $\varrho_c = \varrho_c(M_c, R_c)$, $T_c = T_c(M_c, R_c)$ and $P_c = P_c(M_c, R_c)$ from Eqs. (8)–(10) with $r/R_c = 1$. In the transition layer the chemical composition is homogeneous, radiation pressure can be neglected and T = constant. Then, from Eq. (1), $d \ln P = d \ln \varrho$ and Eq. (2) becomes

$$d \ln \varrho = \frac{G\mu}{\mathcal{R}} \cdot \frac{M_c}{T_c R_c} \cdot d\left(\frac{R_c}{r}\right). \qquad \text{(A 1)}$$

According to Eqs. (9) and (23), $T_c \cdot R_c/M_c = K$ is a constant for all models. Integration of Eq. (A 1) from $r = R_c$ to $r = r_d$ gives

$$\ln \varrho_d - \ln \varrho_c = \frac{G\mu}{\mathcal{R}K} \cdot \left(\frac{R_c}{r_d} - 1\right). \qquad \text{(A 2)}$$

For ϱ_d, we use the value at which the formulae for a perfect gas and for non-relativistic degeneracy give the same value of the electron pressure (Schwarzschild, 1958, p. 60):

$$\varrho_d = D \cdot T_c^{3/2} \qquad \text{(A 3)}$$

($D = \mu_E \cdot 2.4 \cdot 10^{-8}$ g cm^{-3} degree$^{-3/2}$). This gives

$$\frac{3}{2} \ln T_c - \ln \varrho_c - \frac{G\mu}{\mathcal{R}K} \cdot \left(\frac{R_c}{r_d} - 1\right) = -\ln D. \qquad \text{(A 4)}$$

Accordingly, for differential changes of M_c and R_c, one has

$$\frac{3}{2} d \ln T_c - d \ln \varrho_c - \frac{G\mu}{\mathcal{R}K} \cdot \frac{R_c}{r_d} \cdot (d \ln R_c - d \ln r_d) = 0\,; \qquad \text{(A 5)}$$

$d \ln \varrho_c$ and $d \ln T_c$ can be expressed in terms of $d \ln M_c$ and $d \ln R_c$ according to Eqs. (8) and (9); for $d \ln r_d$, we use the M–R relation of white dwarfs

$$d \ln r_d = -\varphi \cdot d \ln M_c \qquad \text{(A 6)}$$

($\varphi > 0$). Then, Eq. (A 5) becomes

$$\left(\frac{3}{2} + \alpha_2 + \frac{G\mu}{\mathcal{R}K} \cdot \frac{R_c}{r_d}\right) d \ln R_c = \left(\frac{3}{2} - \alpha_1 - \varphi \cdot \frac{G\mu}{\mathcal{R}K} \cdot \frac{R_c}{r_d}\right) d \ln M_c\,. \qquad \text{(A 7)}$$

Thus, $d \ln R_c/d \ln M_c$ depends on R_c/r_d, α_1, α_2 and φ.

For a given model, R_c/r_d can be estimated from Eq. (A 4). If we take, for example, a numerical model with intermediate core mass from the equilibrium sequence for $M = 1.4\,M_\odot$, we find:

$M_c = 0.356\,M_\odot$, $R_c = 1.83 \cdot 10^9$ cm,

$T_c = 4.3 \cdot 10^7$ °K, $\varrho_c = 84.5$ g/cm^3.

This gives $K = T_c \cdot R_c/M_c = 1.105 \cdot 10^{-16}$ °K cm/g and, with $\mu = 4/3$, $G\mu/\mathcal{R}K = 9.7$. Then, Eq. (A 4) yields $R_c/r_d = 1.523$ and $r_d = 1.2 \cdot 10^9$ cm. At this point of the numerical model, $M_d = 0.346\,M_\odot$ and the degeneracy parameter is +1.8. Thus, we really have $M_d \approx M_c$ (within 3%) and the transition from medium to strong degeneracy at $r = r_d$. (The degeneracy parameter is −10 at $r = R_c$ and +27 at $r = 0$.) For other models, one obtains even larger values of R_c/r_d. The rather large extension of the transition layer is, of course, due to the high temperature throughout this region.

In Eq. (A 6), φ varies only little in the M_c-range under consideration, and we take $\varphi = 0.5$. Using again the example $\nu = 14$, $n = 2$, $a = 0.1$, $b = -0.8$, one has $\alpha_1 = -3$ and $\alpha_2 = 2.35$. Then, from Eq. (A 7), we get $d \ln R_c / d \ln M_c = -0.16$. This estimation shows already that R_c decreases with increasing M_c and that the relative change of R_c is much smaller than that of M_c. Even the estimated numerical value of $d \ln R_c / d \ln M_c$ is not too bad; from Table 2, one gets for the first two M_c-intervals $d \ln R_c / d \ln M_c = -0.14$ and -0.25, respectively. For large core masses, the radiation pressure should have been taken into account, and this would have resulted in larger absolute values of $d \ln R_c / d \ln M_c$. It is also obvious that R_c / r_d must be larger in a real star (with non-negligible T-gradient inside the core) than in an equilibrium model of the same M_c since the transition layer is hotter in the real star. This difference will increase with increasing M_c, and $|d \ln R_c / d \ln M_c|$ must be smaller in the real star (cf. Fig. 4).

One of the authors (A. Weigert) thanks the staff of the Department of Physics, University of Nebraska, for their generous hospitality during his visit (on leave of absence from University Observatory, Göttingen). Part of the work was supported by National Science Foundation (GP - 9136).

References

Eggleton, P. 1967, *Monthly Notices Roy. Astr. Soc.* **135**, 243.
Giannone, P., Refsdal, S., Weigert, A. 1970, *Astron. Astrophys.* **4**, 428.
Hofmeister, E., Kippenhahn, R., Weigert, A. 1967, *Methods in Computational Physics*, Vol. 7, p. 192. Ed. B. Alder, S. Fernbach and M. Rotenberg. Academic Press, New York, London.
Kippenhahn, R., Kohl, K., Weigert, A. 1967, *Z. Astrophys.* **66**, 58.
Kippenhahn, R., Thomas, H.-C., Weigert, A. 1965, *Z. Astrophys.* **61**, 241.
Kippenhahn, R., Thomas, H.-C., Weigert, A. 1968, *Z. Astrophys.* **69**, 265.
Refsdal, S., Weigert, A. 1969, *Astron. Astrophys.* **1**, 167.
Schwarzschild, M. 1958, Structure and Evolution of the Stars. Princeton University Press.
Schwarzschild, M., Härm, R. 1965, *Astrophys. J.* **142**, 885.
Thomas, H.-C. 1967, *Z. Astrophys.* **67**, 420.
Weigert, A. 1966, *Z. Astrophys.* **64**, 395.

S. Refsdal
Institutt for teoretisk Astrofysikk
Universitetet i Oslo
Postboks 1029
Blindern, Oslo 3, Norway

A. Weigert
Hamburger Sternwarte
BRD-2050 Hamburg 80, Germany